Comparison of LPBF processing of AlSi40 alloy using blended and pre-alloyed powder

Garrard, Rebecca; Lynch, Donal; Carter, Luke N.; Adkins, Nicholas J.E.; Gie, Rodolfe; Chouteau, Estelle; Pambaguian, Laurent; Attallah, Moataz M.

DOI:
10.1016/j.addlet.2022.100038

Document Version
Publisher's PDF, also known as Version of record

Citation for published version (Harvard):
Garrard, R, Lynch, D, Carter, LN, Adkins, NJE, Gie, R, Chouteau, E, Pambaguian, L & Attallah, MM 2022, 'Comparison of LPBF processing of AlSi40 alloy using blended and pre-alloyed powder', *Additive Manufacturing Letters*, vol. 2, 100038. https://doi.org/10.1016/j.addlet.2022.100038

Additive Manufacturing Letters 2 (2022) 100038

Contents lists available at ScienceDirect

Additive Manufacturing Letters

journal homepage: www.elsevier.com/locate/addlet

Comparison of LPBF processing of AlSi40 alloy using blended and pre-alloyed powder

Rebecca Garrard[a], Donal Lynch[a], Luke N. Carter[a], Nicholas J.E. Adkins[a], Rodolfe Gie[b], Estelle Chouteau[c], Laurent Pambaguian[d], Moataz M. Attallah[a,*]

[a] School of Metallurgy and Materials, University of Birmingham, Edgbaston, Birmingham B15 2TT, UK
[b] 235, Rue des Canesteu -ZI La Gandonne, 13300 Salon de Provence, France
[c] Thales Alenia Space, 5 Allée des Gabians, BP 99, 06156 CANNES LA BOCCA Cedex, France
[d] European Space Agency ESA-ESTEC, Material Mechanics and Processes Section, Keplerlaan 1, P.O. Box 299, NL-2200 AG Noordwijk ZH, The Netherlands

ARTICLE INFO

Keywords:
In-situ alloying
Low CTE alloy
Feedstock comparison
Hypereutectic AlSi alloy
Laser powder bed fusion
Additive manufacturing

ABSTRACT

Elemental powders or pre-alloyed powders can be blended to form a powder stock with new compositions. In-situ alloying of blended powder mixtures during LPBF processing speeds up the alloy development process as it allows composition adjustment. Pre-alloyed powder is typically used in industrial settings to ensure consistency of the built material, whereas blended powders are used to experiment with new alloy compositions. In this research, we compare a range of binary alloy compositions built from blended elemental powder and pre-alloyed powder to evaluate how the feedstock powder affects the built material. The alloy is a lightweight alloy with a low coefficient of thermal expansion, comprised of Al and Si. The following compositions were formed by mixing pure Al and Si powder: AlSi38, AlSi40 and AlSi42, and pre-alloyed AlSi40 powder was also used.

Parametric studies were performed for both the blended and pre-alloyed powders. It was found that the optimum process parameters for the blended and pre-alloyed powder were different. The line energy for pre-alloyed powder was selected to be 0.150 J/mm (300 W, and 2000 mm/s) which yielded a density of 99.5% of the theoretical density. The optimal density for the blended powders was 99.07-99.16% which was also achieved with 0.150 J/mm (375 W, 2500 mm/s). The alloys are brittle, with Young's modulus 86-99 GPa. Coefficient of thermal expansion (CTE) reduced with increasing Si content, material built from pre-alloyed powder had 5% higher CTE than material built from blended powder.

1. Introduction

Hypereutectic AlSi alloys are a focus of research interest due to the low coefficient of thermal expansion (CTE) that can be achieved through high silicon content. Laser powder bed fusion (LPBF) has expanded the ability to process these alloys which were typically limited to processes such as spray deposition and casting. LPBF processing with blended powders has been used to develop and optimise the compositions of novel hypereutectic AlSi alloys. In this study, an alloy with low CTE and low density is developed, the in-situ alloying method can be used to further tailor the CTE and mechanical properties to specific applications such as components for aerospace. This approach allows a more flexible approach to alloy development as the concentrations of the alloy components can be quickly tailored without incurring additional costs, and delays and costs caused by manufacturing pre-alloyed powders are eliminated. However, in industrial settings pre-alloyed powders are typically used. This work evaluates the validity of in-situ alloying for material development, by assessing how the powder alloying method affects the thermal and mechanical properties of LPBF built material.

1.1. Background to hypereutectic AlSi alloys

Hypereutectic AlSi alloys have been developed to combine and balance the desirable low thermal expansion of Si combined with the high specific strength of Al. These alloys were originally developed for packaging circuitry, for use in avionics and space applications, and they were processed by spray forming [5]. AlSi alloys have a eutectic point at 11.7 wt% Si [1]. Liu et al [14] found in a study of AlSi20, with the addition of strontium, alloys with greater Si content require rapid cooling to avoid segregation of large Si-phase particles. Research into processing hypereutectic AlSi alloys through LPBF and exploiting the high cooling rates associated with the technology has been performed since 2014 [15]. In this study, the as-built microstructure of AlSi20 produced from

* Corresponding author.
E-mail address: M.M.Attallah@bham.ac.uk (M.M. Attallah).

https://doi.org/10.1016/j.addlet.2022.100038
Received 5 January 2022; Received in revised form 16 February 2022; Accepted 17 February 2022

pre-alloyed powder was found to be comprised of supersaturated Si in an Al matrix, with fine particles of segregated Si.

1.2. Blended powder

Pure Al and Si powders respond differently to the energy input from the laser. The reflectivity of Al is significantly greater than that of Si, and Al has a lower melting point compared with Si, 660.3 °C and 1404 °C respectively. Evaporation of Al is a concern with the LPBF processing of AlSi alloys. Hanemann et al [4] found that higher Si content increased the energy input required to achieve densities ≥99%. They fabricated AlSi25 and AlSi50 by blending AlSi10Mg powder (39 μm mean diameter) with pure Si powder (44 μm mean diameter) and found reasonable mixing although some Si particles did not melt. The CTE of the built material was found to reduce by 0.2×10^{-6} 1/K per wt% Si. Al evaporation can be exacerbated by the increased temperatures required to melt elemental Si powder, Kang et al reported 10 wt% loss of Al when processing AlSi50 produced from blended elemental powders [8].

It is expected that the increased temperatures required for elemental powders will be reflected in an increased heat input required to achieve satisfactory densities with blended powders compared with pre-alloyed. Jia et al [6] processed AlSi50 from blended and pre-alloyed powder and found that blended AlSi50 achieved full density within the line energy range 0.227-0.342 J/mm while pre-alloyed AlSi50 was processed with bulk parameters, which equated to line energy of 0.22 J/mm; the resultant density is not reported. Conversely, Kang et al [9] found that for AlSi12, a lower energy density is required to process blended powder than pre-alloyed powder.

For the hypereutectic AlSi alloy under consideration, there is a large and nearly equal concentration of alloying elements and powder particles of similar sizes and characteristics have been used which minimises risks of inconsistent composition. In some studies, the elemental Si powder is significantly finer than the Al powder, for example, AlSi12 was produced from a blend of Al with a mean particle size of 42 μm and Si powder with a mean size of 6 μm [9] and AlSi12 (mean size 30 μm) has been blended with 7.4 wt% Si (mean size 6 μm) [10]. It is argued that for small concentrations of alloying elements, it is more appropriate to use a finer powder particle size. Satelliting a large particle with finer particles of alloying elements was compared to powder blending and pre-alloyed powder in a study of Ti6Al4V by Simonelli et al [18].. A limitation of this study was that the size of the V particles was large relative to their concentration in the alloy. It was found that the satellited powder yielded the microstructure most like that of material built from pre-alloyed powder, however, the process parameters were not optimised for each feedstock powder. The blended powder was found to yield inhomogeneity to be addressed by post-processing heat treatment.

Kang et al [11]. investigated formation of microstructure of AlSi50 built from blended elemental powders. They found that primary Si nucleates from the melt and Marangoni forces drive the Si to the edges of the melt pool. The centre of the melt pool solidifies more slowly, with a reduced Si content. Primary Si that forms in the centre of the melt pool is larger than the primary Si at the edges of the meltpool. The size of the primary Si is affected by the laser power, laser power above 210 W with a scan speed of 500 mm/s was found to increase the Si particle size due to the reduced cooling rate. In a study of AlSi18, Kang et al [10] blended AlSi10 and pure Si, the microstructure of the built material was comprised of nano- and irregular micro- Si (which was partially melted Si particles). Increasing the laser power eliminated the partially melted particles, and the shape of the Si particles became more spherical. The size change of primary Si was measured in AlSi50 built from blended powder by Kang et al [8]. The distribution of primary Si was homogeneous, and when the laser power was 290 W, the mean primary Si particle size was 3.12 μm, increasing to 6.17 μm at 320 W. Higher laser powers result in a larger melt pool and slower cooling rates, allowing for Si segregation.

1.3. Pre-alloyed powder

Fewer studies have been performed on pre-alloyed hypereutectic AlSi alloy powders than on blended powder; this is likely to be due to the lack of commercially available alloys. Pre-alloyed powder reduces the risk of inhomogeneity in built material. Roberts et al [17]. reported that material built from pre-alloyed powder may be more vulnerable to cracking than a blend of Al and Si powder, however, the Si was not fully melted in their LPBF process, thus they formed an Al matrix around Si particles. When processing pre-alloyed AlSi40, Erberle et al [2] reported extensive cracking, despite using a heated powder bed. AlSi40 is a brittle material, with 0.6 ± 0.3% extension to failure in the as-built condition, built in the horizontal direction. Process parameters were found to be significant in controlling cracking; reducing the length of scan vectors and changing the sample geometry reduced cracking [2]. Mueller et al [16] report 1.1% elongation and mean UTS of 279 MPa of LPBF produced AlSi40 samples which were hot isostatic pressed (HIP) and heat treated. For AlSi12, Kang et al [9] reported an inverse relationship between scan speed and tensile strength and ductility. Comparing tensile properties of AlSi12 built from pre-alloyed and blended powder revealed that the blended material has lower ultimate tensile strength, but higher ductility [9].

Kimura et al [13] used pre-alloyed AlSi powder with a range of compositions, alloys with 7-20 wt% Si were found to require lower energy input than 0-4% wt% Si. This difference in energy requirement was attributed to the higher flowability of the increased Si alloys.

1.4. Properties of AlSi alloys

Increasing the Si content of hypereutectic AlSi alloys increases the materials wear resistance [12] and thermal stability [4]. For AlSi40 built from pre-alloyed powder, CTE is reported to be 13.3×10^{-6} $mm^{-1}K^{-1}$ at 20 °C after heat treatment and HIP [2]. Jia et al [6] studied the thermal expansion of as-built AlSi50, in the temperature range 300-450 K, the CTE is minimised by the supersaturated Si in Al. Heat treatment caused the Si to precipitate. There is a peak in CTE around 500-600 K, caused by segregation of Si from the Al matrix.

Heat treating AlSi50 built from blended powder over 723 K caused Si to diffuse from the matrix, the resultant microstructure was globules of pure Si surrounded by Al [7]. When the alloy is heated to close to the eutectic point (823 K) a significant increase in porosity at the boundaries between the Al and Si regions was also found to occur. Annealing has been used on LPBF built AlSi20 at 473 K, 573 K and 673 K by Ma et al [15]. These heat treatments were found to reduce the yield and UTS but increase the ductility. Annealing causes the primary Si particles to increase in size, which increases the distance between them. The primary Si acts to limit the movement of dislocation, so the greater space between the particles allows greater movement of dislocations [15].

In this work, AlSi38, AlSi40 and AlSi42 were produced by LPBF using blended elemental powders and compared to AlSi40 pre-alloyed powder. To investigate the difference between the powder feedstocks and resultant material, process parameter optimisation was performed and the microstructure, CTE and tensile properties were evaluated.

2. Material and methods

2.1. Feedstock powder

TLS Technik GmbH supplied both the pre-alloyed and elemental powders produced by gas atomization. Powder morphologies were assessed with SEM images (Error! Reference source not found. a-c). The three powders were of similar size and shape with large, near-spherical particles with many very fine particles. The fine particles exhibit behaviour where the surface Van der Waals forces are not overcome by gravitational forces resulting in clustering or satelliting the larger particles. Size analysis showed that they all have a bimodal distribution

Table 1
Particle size analysis results from laser diffraction and flowability measurements.

	Particle Size, μm			Apparent Density		Tap Density		Hausner ratio
	D10	D50	D90	g/cm^3	%	g/cm^3	%	
Al	24.4	46.9	82.9	0.96	35.5	1.12	41.5	1.18
Si	19.6	40.0	67.5	1.12	48.1	1.39	59.7	1.24
AlSi38 B	22.7	44.1	77.7					
AlSi40 B	22.6	43.9	77.4	1.31	51.3	1.54	60.4	1.17
AlSi42 B	22.6	43.8	77.1					
AlSi40 PA	19.6	48.0	83.8	1.32	51.8	1.56	61.2	1.18

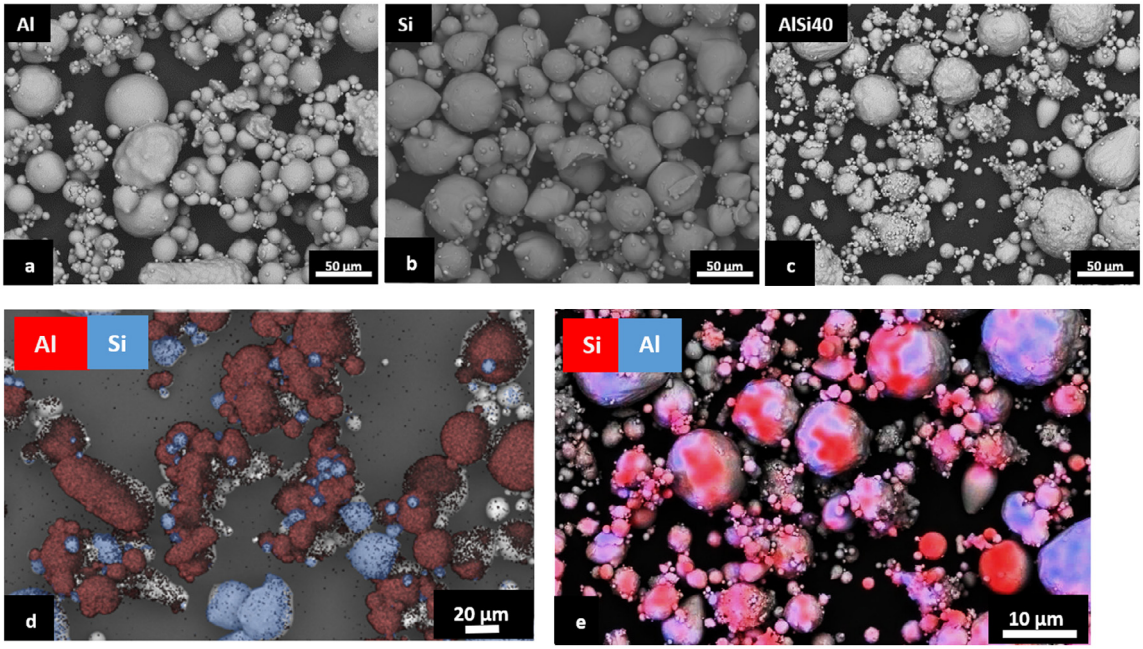

Fig. 1. a c BSE+SE SEM micrographs showing the three feedstock powders; (a) pure Al, (b) pure Si, and (c) pre-alloyed AlSi40. d) EDX map of blended AlSi38 and e) EDX map of pre-alloyed AlSi40 powder.

due to the presence of fine particles, with a small peak below 10 μm, and a large peak around 70-80 μm (Fig. 2). In the Si powder, some fractured particles were observed, likely relating to the brittleness of the material. The Si powder has a slightly smaller and narrower size distribution. Flowability of the elemental and pre-alloyed powders was assessed through the calculation of the Hausner ratio (Table 1). The upper threshold for flowability for LPBF is a Hausner ratio of 1.25. For pure Si, the Hausner ratio is 1.24 which is close to the flowability limit, with blended and pre-alloyed powders both having better and similar flowability (1.17-1.18).

The elemental powders were combined in a ratio of 60:40 Al:Si by weight in an oxygen-depleted environment, and mixed by tumbling on rollers for 8 hours. Homogeneous mixing was confirmed by scanning electron microscopy (SEM, Hitachi TM3000) and energy-dispersive x-ray spectroscopy (EDX) mapping of a mixed powder sample (Error! Reference source not found. d). Elemental distribution in the pre-alloyed powder is shown in Fig. 1e.

Inductively coupled plasma atomic emission spectroscopy was used to measure the composition; the pre-alloyed powder was 60.1 wt.% Al and 39.4 wt.% Si and the contamination levels were acceptable. The elemental powders were found to be 99.8 wt.% pure. The oxygen content of all powders was below 0.1 wt%.

2.2. LPBF Processing

A Concept Laser M2 LPBF machine was used to process the blended and pre-alloyed powders. It is equipped with a 400 W continuous-wave laser. Parametric studies were performed; an array of 25 coupons (10 × 10 × 10 mm) was built with varying laser power and scan speed over a range of 300-400 W and 1250 – 2500 mm/s. The same parameters were used for the pre-alloyed and blended powders, although an additional parameter study was performed for the pre-alloyed powder with a power and scan speed range of 175-300 W and 1500 – 2500 mm/s. Line energy was calculated for the parameter sets using Eq. 1, where E is line energy (J/mm), P is laser power (W), and v is scan speed (mm/s). The island scanning strategy was used with 5 mm islands, island overlap of 22.5 μm, hatch spacing of 75 μm, and 30 μm layer thickness. The parts were built on an Al alloy build plate and were removed from the plate using wire electric discharge machining (EDM).

$$E = \frac{P}{v} \tag{1}$$

2.3. Heat treatment development

Four heat treatments were selected from literature; Kang et al [7]. measured the effect of different heat treatments of LPBF processed AlSi50, with temperatures ranging from 300 600 °C for 2 hrs. They reported that heat treatment at 300 °C reduces the residual stress in the built samples without a significant change in the microstructure, while heat treatments above 500 °C induce porosity at the interfaces between the silicon and aluminium. Ma et al [15]. measured the influence of heat treatment on AlSi20. A significant increase in ductility was seen with temperatures above 300 °C, this is more of a concern with the alloys in this work due to the higher proportion of silicon.

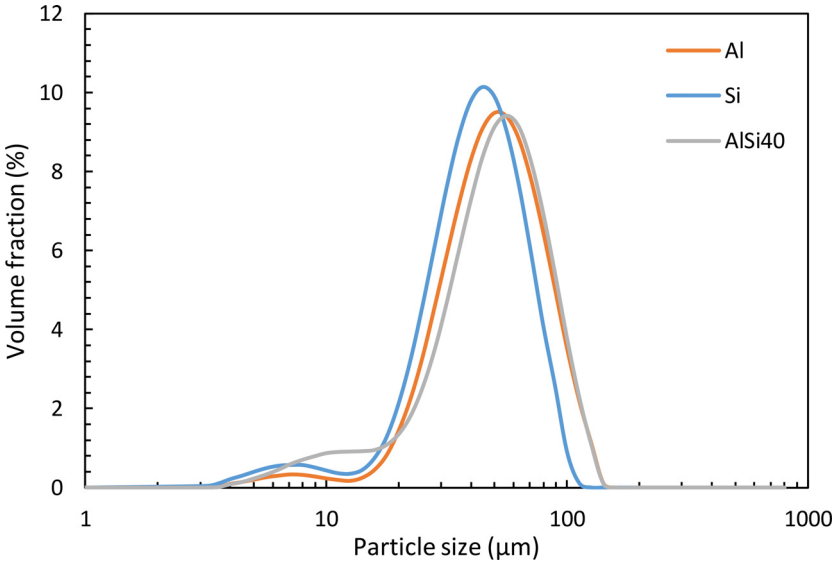

Fig. 2. Size distribution of powder used in this study measured by laser size diffraction.

Table 2
Heat treatments.

	HT1	HT2	HT3	HT4
Temp (°C)	250	250	350	400
Time (hr)	12	8	8	8

It was decided to test temperature between 250 °C and 400 °C, where material should have a change in microstructure to allow for an increase in ductility and below the temperature which induces porosity. 8 hrs was selected for the duration with one set of samples being treated for 12 hrs to see if there is a significant difference. Heat treatment conditions are provided in Table 2. HT2 was selected based on CTE and tensile values of the blended samples.

2.4. Evaluation of built material

The parametric study aimed to identify the parameters that resulted in the highest density blocks. The density of the blocks was measured using the Archimedes method with ethanol. After the density was measured, the samples were heat-treated. Relative density was calculated as a ratio of the measured density of a block to the theoretical density of the alloy. Selected blocks were sectioned and polished to enable microstructural evaluation with SEM using a combined backscatter electron and secondary electron imaging mode (BSE+SE). Tensile test bars were machined from heat-treated cylindrical rods to the TETRE 160 Taper tensile sample geometry (cylindrical dogbone with reduced section diameter 4 mm and 16 mm length). Tensile testing was performed according to standard ASTM E8-16a. CTE samples were machined from material built in the vertical and horizontal directions, and tested using a Perkin Elmer TMA7 dilatometer over a temperature range of 303 to 403 K.

3. Results and discussion

3.1. LPBF parameter development

A preliminary trial on blended powder (AlSi38) found that line energy <0.150 J/mm resulted in lack-of-fusion defects and failure to completely melt the silicon particles (Fig. 3); therefore this was selected as the lower limit for the parameter study. The line energy was varied in the range 0.15-0.32 J/mm; the process parameters are shown in Table 3.

For the blended powders, there is an inverse relationship between line energy and Archimedes density. All three alloys had the highest density in the range 0.15-0.187 J/mm. The maximum densities were 99.07-99.16% of the theoretical density. All samples exhibited keyhole porosity; this could be caused by the difference in thermal properties between the elemental powders. Low line energy is likely to cause lack-of-fusion pores, and at higher energies keyhole porosity is more likely to occur. The blended AlSi40 achieved higher densities than the AlSi40 PA with an average difference of 0.19%, Table 3 . The maximum density for AlSi40 PA was 98.85% and was achieved when processing with 0.150 J/mm, at this line energy AlSi40 (blend) was 99.16% dense.

None of the parameters in the first process parameter build for AlSi40 PA (Table 3) yielded the target density of 99%. As the highest densities were achieved with the lowest line energies and the pre-alloyed powder wasn't encumbered by un-melted silicon defects, a second parameter study was performed with line energies in the range 0.070-0.183 J/mm. Higher densities, up to 99.87%, were achieved with lower energy input. However, cracking occurred at the lower end of the energy range of the parameters, 0.700-0.129 J/mm (Fig. 4). There is not a clear threshold for the onset in cracking as the range 0.110-0.129 J/mm some samples cracked, and others didn't. Hanemann et al [4] reported that for AlSi25 and AlSi50 produced from blended powders that cracking occurred when using high scanning speed and low laser power. The cracking seen in the pre-alloyed samples may relate to the increased density of the samples as porosity may act to relieve stress.

The optimal processing parameters for the pre-alloyed powder were selected to be with 2000 mm/s scan speed and 300 W laser power (0.150 J/mm line energy), these parameters yielded 99.53% density and were outside of the cracking parameter window. For the blended powders, the optimum parameter set was: 375 W and 2500 mm/s (0.150 J/mm) as sufficient density in the three alloys was achieved. For the blended alloys, Mueller et al [16]. found optimum parameters for AlSi40 PA with 0.126 J/mm but they also used a heated bed of 170 °C. Using computed tomography, the density was measured as 99.6%, but only 96.8% when measured by the Archimedes method. Post-process heat treatment and HIP can increase density, Erberle et al [2]. achieved 99.7% density of pre-alloyed AlSi40 using these processes, although the LPBF parameters and as-built density are not reported. Cracking was also reported to be especially problematic for horizontally built material and was affected by the process parameters.

Hanemann et al [4] produced AlSi50 from blended powders with 99.90 ± 0.05% density with line energy of 0.233 J/mm, the increased Si content requires higher energy to melt. Pre-alloyed AlSi50 was pro-

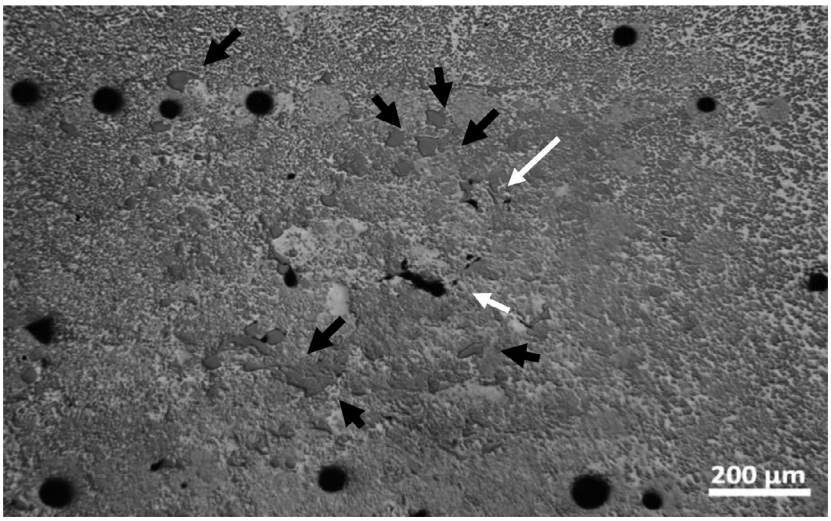

Fig. 3. Optical micrograph of AlSi38 produced from blended powders (E= 0.100 J/mm). The black arrows indicate unmelted Si particles and the white arrows indicate lack of fusion defects.

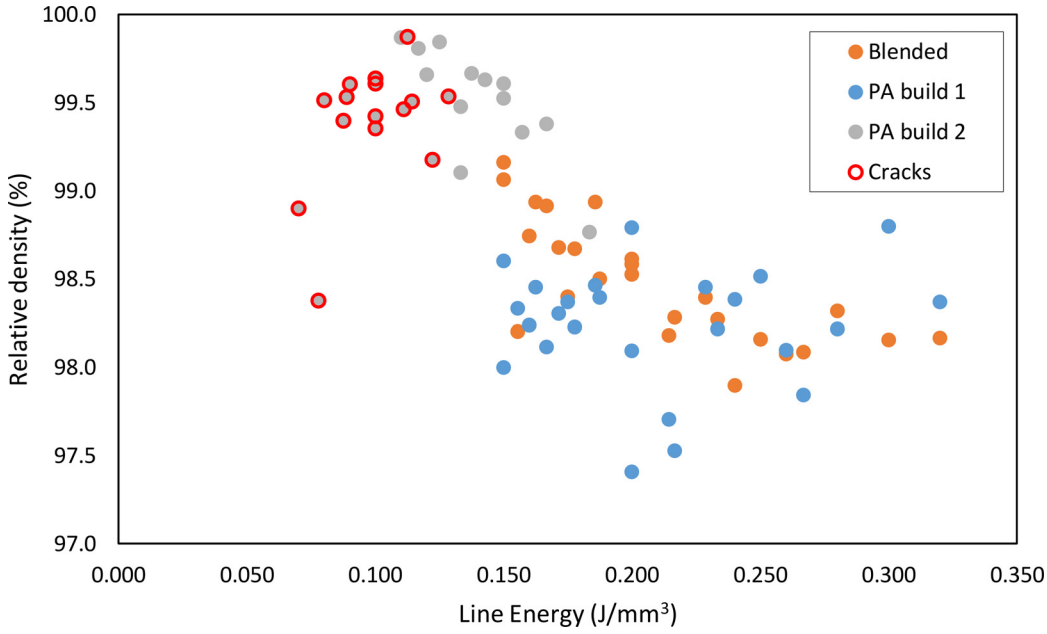

Fig. 4. Archimedes density results of AlSi40 produced from blended and pre-alloyed powder. Samples that were cracked are highlighted in red, all the cracked samples occurred in the second pre-alloyed build.

cessed with line energy of 0.220 J/mm by Jia et al [6], although the resultant density is not stated. In the current study, it has been found that higher densities can be achieved with lower energy input for the pre-alloyed powder, which is consistent with the findings in the literature.

3.2. Evaluation of built material

3.2.1. Microstructural analysis

Microstructural analysis was performed on AlSi40 B and AlSi40 PA to compare the alloying methods. Before heat treatment, the microstructure of the AlSi40 PA (Fig. 5a) shows irregular polygon-shaped crystals of primary Si in an AlSi12 matrix. This microstructure was also observed in AlSi40 formed by laser cladding [3]. Grigoriev et al [3] describe this microstructure as primary Si crystals which nucleate from the undercooled melt, α-Al halos form around the Si crystals, and eutectic AlSi12.6 forms the matrix.

Within the matrix in Fig. 5a and 5c, there are discontinuous white seams, which are likely to be located at the boundaries of the solidifying grains. The bright appearance of the seams suggests that they are an inclusion such as iron or oxides and the increased presence is consistent with the level of contaminants in the pre-alloyed powder. The composition of the seams could not be analysed by EDX as it was too fine. AlSi40 B in the as-built condition has a similar appearance to that of AlSi40 PA, but the Si phase crystals are around 18% larger. This indicates that alloying elements are more intimately mixed within the material processed from pre-alloyed powder than when processing a mixture of two different powders. The microstructure obtained from blended powder doesn't show any unmelted particles or evidence of incomplete mixing.

In-situ alloying has benefitted from a combination of factors; the high concentrations of Al and Si, similar powder characteristics, and the simplicity of the Al-Si phase diagram. The single eutectic of Al-Si means that localised variations in composition will not form metastable phases. Although Al has a lower melting temperature than Si, it has higher reflectivity. The similar powder particle size and close to 50:50 mixing limit the potential of inhomogeneity in the meltpool.

Fig. 5b and 5d show that heat treatment softens the boundaries between the Si-rich and Al-rich phases, with Si diffusing into the α-Al cre-

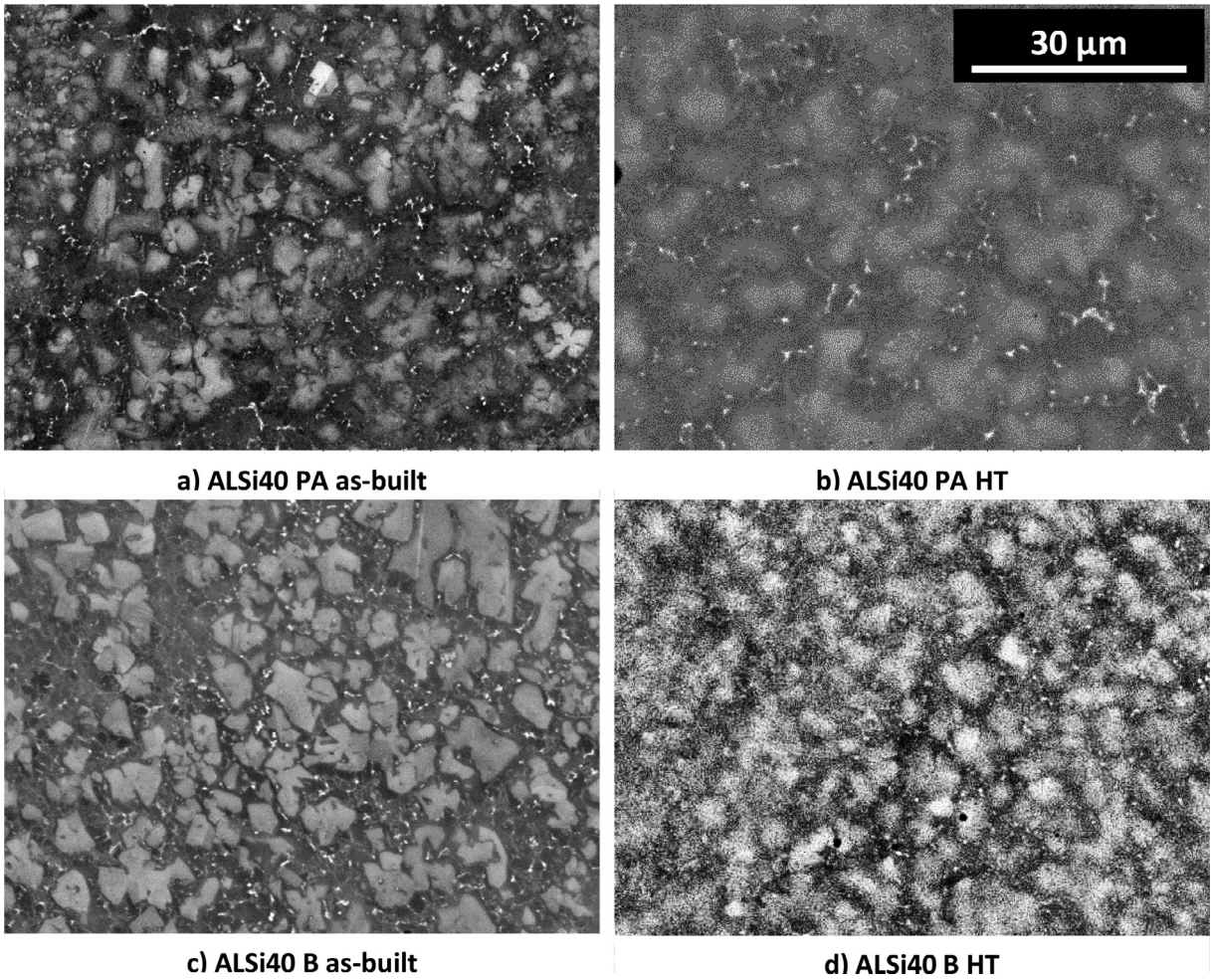

Fig. 5. SEM (BSE+SE) images of the microstructure of material built from pre-alloyed and blended AlSi40 (perpendicular to the build direction), in the as-built and heat-treated conditions. AlSi40 PA was processed with 2000 mm/s scan speed, 300 W laser power, 75 µm hatch space, and 30 µm layer thickness. AlSi40 B was processed with 2500 mm/s scan speed, 375 W, 75 µm hatch space, and 30 µm layer thickness. The heat treatment used was 250°C for 8 hours.

ating ghost structures of the previously large Si precipitates. The size reduction of the Si precipitates should increase the ductility due to the brittleness of pure Si, and increases the homogeneity of the microstructure. In HT AlSi40 PA (Fig. 5b), the bright inclusion of contaminants is less pronounced, potentially due to diffusion or recrystallization during heat treatment. An interconnected network of eutectic AlSi is present. These veins of eutectic AlSi are present in AlSi40 B, although it is less evident after heat treatment. Kang et al [7] reported that from the phase diagram the microstructure of AlSi50 should be primary Si in a lamellar eutectic matrix, thought the non-equilibrium cooling of the LPBF process could disrupt this formation. The as-built material in their study had a similar microstructure to Fig. 5 .a and b, although the primary silicon had a more rounded morphology, this difference may have been caused by the powder bed heating (127 °C) reducing the cooling rates. It was shown that heat-treating AlSi50 at 550 °C for 2h followed by a water quench resulted in segregation of the Al and Si. The heat treatment used in the present study used a much lower temperature and appears to have promoted some diffusion between the microstructural phases (Table 3).

3.2.2. Mechanical property analysis

Results of tensile testing are shown in Table 4. All the samples tested were brittle, this can be seen in the low elongation of both the pre-alloy and blended samples. A typical stress-strain graph is shown in Fig. 6. Increasing the Si content increases Young's modulus, UTS and 0.2% OYS at the expense of elongation. Si is hard but brittle, in the microstructure large regions of pure Si were seen, which increasingly influence mechanical performance with higher Si content.

Comparing AlSi40 B and AlSi40 PA, the pre-alloy has superior performance for all measures except elongation, although the difference between the blend and pre-alloy is ≤10% for all measures. In the parameter study, the optimised parameters yielded 99.16% density for AlSi40 B, and 99.53% for AlSi40 PA. The increased density of the pre-alloy may contribute to its superior mechanical properties. These findings are similar to a study of AlSi12, where pre-alloyed powder resulted in superior UTS, but inferior elongation to blended powder ([7]b).

Eberle et al [2]. performed mechanical testing on AlSi40 built vertically from pre-alloyed powder, after heat-treatment (6h at 400 °C) and HIP (400 °C for 2h at 1950 bar in Ar) their results are inferior to both AlSi40 B and AlSi40 PA in this study, except for the UTS of AlSi40 B. However, they found that the horizontal as-built material outperformed vertically built material. They do not provide any micrographs for comparison.

3.2.3. Coefficient of thermal expansion

CTE results (Table 5) show that the alloys in this study have low thermal expansion. When designing components, the effect of build orientation on CTE is an important consideration. CTE was measured on heat-treated samples built in the vertical and horizontal build direction. Increasing the Si content in the blended samples decreased the CTE. In

Table 3
Relative densities (%) of the parameter studies for pre-alloyed and blended powder.

AlSi38 B

Power (W) \ Speed (mm/s)	1250	1500	1750	2000	2250	2500
300	98.07	98.27	99.07	98.83		
325	98.20	98.35	98.48	98.59		
350	97.96	98.59	98.43	98.83	98.23	
375	98.14	98.48	98.10	98.39	98.61	98.73
400	98.01	98.23	97.87	98.41	98.86	98.68

AlSi40 B

Power (W) \ Speed (mm/s)	1250	1500	1750	2000	2250	2500
300	97.90	98.58	98.68	99.06		
325	98.08	98.28	98.94	98.94		
350	98.32	98.27	98.61	98.40	98.20	
375	98.16	98.16	98.18	98.50	98.91	99.16
400	98.17	98.09	98.40	98.53	98.67	98.75

AlSi42 B

Power (W) \ Speed (mm/s)	1250	1500	1750	2000	2250	2500
300	97.83	98.86	98.89	99.14		
325	98.22	98.33	99.11	98.79		
350	98.07	98.38	98.93	99.06	98.61	
375	97.80	98.23	98.73	98.84	99.04	98.87
400	97.96	97.77	98.12	98.77	98.68	98.79

AlSi40 PA

Power (W) \ Speed (mm/s)	1250	1500	1750	2000	2250	2500
300	97.75	98.26	98.84	98.85		
325	98.14	98.05	98.44	98.50		
350	97.57	98.15	98.42	98.51	98.65	
375	97.45	98.29	98.27	98.38	98.42	98.56
400	97.89	98.16	98.35	98.26	98.50	98.43

Table 4
Mechanical properties of heat-treated samples, tested in the vertical build direction. For the blended samples the values are the mean of 5 results, and for AlSi40 PA 7 results were used.

	Young's modulus GPa	0.20% OYS MPa	UTS MPa	Elongation after fracture %
AlSi38 B	86 ± 2	208 ± 2	311 ± 4	1.4 ± 0.9
AlSi40 B	90 ± 8	214 ± 3	283 ± 35	1.5 ± 0.8
AlSi42 B	91 ± 2	236 ± 8	327 ± 8	0.1 ± 0.1
AlSi40 PA	99 ± 7	219 ± 4	310 ± 11	1.1 ± 0.5

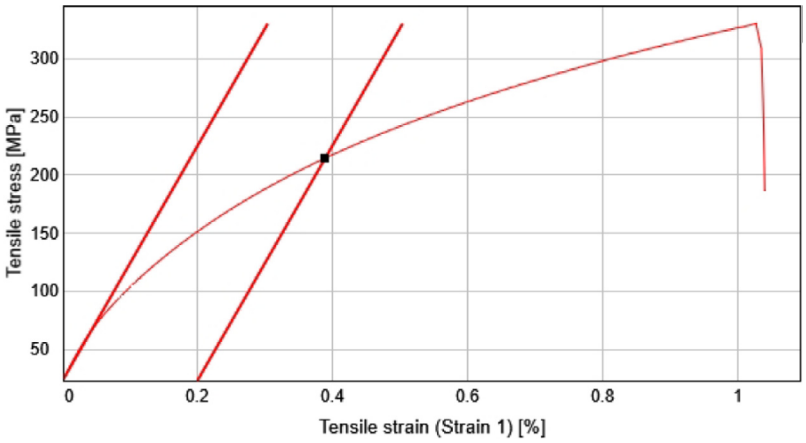

Fig. 6. Typical stress-strain graph of HT AlSi40 PA. The tensile sample was processed with 2000 mm/s scan speed, 300 W laser power, 75 µm hatch space, and 30 µm layer thickness. The heat treatment used was 250°C for 8 hours.

Table 5
CTE values for hypereutectic AlSi alloys produced by LPBF. B indicates blended feedstock powder and PA indicates pre-alloyed powder. Asterisks indicate Si wt% added to AlSi10Mg.

Si content, wt.%	CTE, × 10^{-6} m.$m^{-1}K^{-1}$		Powder type	Condition	Temperature, °C	Source
	H build direction	V build direction				
25*		17.50	B	As-built	100	[4]
38	13.92	14.24	B	HT	30-130	
40	13.45	13.02	B	HT	30-130	
40		13.30	PA	HT+HIP	20	[2]
40	13.55	14.14	PA	HT	30-130	
40		13.33	PA	HT+HIP	20	[16]
42	12.83	12.56	B	HT	30-130	
50*		13.78	B	As-built	100	[4]

horizontally built material the CTE reduces by 0.24×10^{-6} $m.m^{-1}K^{-1}$ per wt% Si. There is a less clear relationship between Si content and CTE for vertically built material due to scatter in the results, CTE reduces at a rate of 0.42×10^{-6} $m.m^{-1}K^{-1}$ per wt.% Si. For AlSi38 B the vertical CTE is higher than the horizontal, but for AlSi40 B and AlSi42 B this is reversed. For each alloy the vertical and horizontal CTE values are 2-3.2% different.

The samples built from AlSi40 B have lower thermal expansion than AlSi40 PA. For both powder types, there is a small difference in CTE measured in different directions. For AlSi40 PA, there is a difference of 0.597×10^{-6} $m.m^{-1}K^{-1}$ with the vertical direction having the greatest CTE. For AlSi40 B, the horizontal direction has the highest CTE, and the difference is 0.443×10^{-6} $m.m^{-1}K^{-1}$. AlSi40 PA CTE is 5% lower than AlSi40 B; this could be due to the increased porosity in the blended material.

The results obtained in this study agree with results from the literature as shown in Table 5. Erberle et al [2] and Mueller et al [16] both measured CTE of LPBF produced AlSi40 from pre-alloyed powder and heat-treated and HIPed. Their CTE values are slightly higher than AlSi40 B. Hanemann et al [4] found that for AlSi10Mg+40Si, CTE reduces by 0.2×10^{-6} $m.m^{-1}K^{-1}$ per wt.% Si over a temperature range of 50-100 °C, therefore the CTE of AlSi40 is estimated as $\sim 16 \times 10^{-6}$ $m.m^{-1}K^{-1}$ although this is a narrower temperature range than was used in this study. The Si crystals act to constrain the thermal expansion, and the finer the crystals are, the more effectively they limit thermal expansion [4], so the diffusion caused by the heat-treatment may increase this effect.

4. Conclusions

In this study, low CTE alloys have been effectively synthesised from blended powder and compared to a pre-alloyed feedstock powder. All three blended alloys (AlSi38, AlSi40 and AlSi42) were processed with the same LPBF process parameters to achieve density >98.7%. AlSi40 PA achieved a density of 99.8% with the same energy input, but with higher scan speed and laser power. Parameters within the processing window of the blended powder resulted in lower densities when processing the pre-alloyed material, which could relate to differences in laser absorption of the elemental powders and levels of evaporation of Al. The pre-alloyed powder was found to be susceptible to cracking during LPBF processing. Full mixing of alloy components was seen in the samples built from blended powder. There is little difference in the as-built microstructure from the blended and pre-alloyed powder. Heat treatment was found to cause diffusion between the primary Si, α-Al and eutectic AlSi matrix.

In-situ alloying was successful in part due to the phase diagram of Al-Si as there was no risk of unfavourable phased forming. Other alloy systems that this could be applicable to include Cu-Ni, and Mo-Nb. In more complex alloy systems such as Al-Cu, localised concentration variations in the melt pool could lead to the formation of unfavourable phases.

Mechanical test results show that these alloys are brittle and increasing the Si content to 42 wt.% resulted in an elongation of 0.1%. and the Young's modulus for the alloys was 86-99 GPa and the UTS was 283-327MPa. AlSi40 PA outperformed the tensile properties of AlSi40 B (except for elongation), although the difference is less than 10%. CTE reduced with increasing Si content, material built from pre-alloyed powder had 5% higher CTE than material built from blended powder.

Overall, these results indicate that for hyper-eutectic AlSi alloys, blended elemental powder and pre-alloyed powder feedstocks yield similar materials. Thus, blended powders can be used to assess the printability and properties of novel alloys in LPBF.

Declaration of Competing Interest

The authors declare that they have no known competing financial interests or personal relationships that could have appeared to influence the work reported in this paper.

Acknowledgements

This work was supported by the European Space Agency (ESA): Additive manufacturing of Aluminium-Silicon alloys with high silicon content (AlSix).

References

[1] Cornell, R. & Bhadeshia, H., n.d. Aluminium-Silicon Casting Alloys. [Online] Available at: https://www.phase-trans.msm.cam.ac.uk/abstracts/M7-8.html
[2] S. Eberle, A. Reutlinger, B. Curzadd, M. Mueller, M. Riede, C. Wilsnack, A. Brandão, L. Pambaguian, A. Seidel, E. López, F. Brueckner, Additive manufacturing of an AlSi40 mirror coated with electroless nickel for cryogenic space applications, in: Proceedings of the International Conference on Space Optics—ICSO 2019, 11180, International Society for Optics and Photonics, 2019.
[3] S.N. Grigoriev, T.V. Tarasova, G.O. Gvozdeva, S. Nowotny, Structure formation of hypereutectic Al-Si-alloys produced by laser surface treatment, J. Mech. Eng. 60 (6) (2014) 389–394.
[4] T. Hanemann, L.N. Carter, M. Habschied, N.J. Adkins, M.M. Attallah, M. Heilmaier, In-situ alloying of AlSi10Mg+Si using selective laser melting to control the coefficient of thermal expansion, J. Alloys Comp. (2019) 8–18.
[5] D. Jacobson, Lightweight electronic packaging based on spray formed Si-Al, Powder Metallurgy (2000) 200.
[6] Y.D. Jia, P. Ma, K.G. Prashanth, G. Wang, J. Yi, S. Scudino, F.Y. Cao, J.F. Sun, J. Eckert, Microstructure and thermal expansion behaviour of Al-50Si synthesized by selective laser melting, J.Alloys Comp. 699 (2017) 548–553.
[7] N. Kang, P. Coddet, M.R. Ammar, H. Liao, C. Coddet, Characterization of the microstructure of a selective laser melting processed Al-50Si alloy: Effect of heat treatments, Mater. Charact. 130 (2017) 243–249.
[8] N. Kang, P. Coddet, C. Chen, Y. Wang, H. Liao, C. Coddet, Microstructure and wear behaviour of in-situ hypereutectic Al-high Si alloys produced by selective laser melting, Mater. Design (2016) 120–126.
[9] N. Kang, P. Coddet, L. Dembinski, H. Liao, C. Coddet, Microstructure and strength analysis of eutectic Al-Si alloy in-situ manufactured using selective laser melting from elemental powder mixture, J. Alloys Comp. (2017) 316–322.
[10] N. Kang, P. Coddet, H. Liao, T. Baur, C. Coddet, Wear behavior and microstructure of hypereutectic Al-Si alloys prepared by selective laser melting, Appl. Surf. Sci. 378 (2016) 142–149.
[11] N. Kang, P. Coddet, H. Liao, C. Coddet, Macrosegregation mechanism of primary silicon phase in selective laser melting hypereutectic Al - high Si alloy, J. Alloys Comp. 662 (2016) 259–262.
[12] N. Kang, M.E. Mansori, A new insight on induced-tribological behaviour of hypereutectic Al-Si alloys manufactured by selective laser melting, Tribol. Int. (2019) 1–6.
[13] T. Kimura, T. Nakamoto, M. Mizuno, H. Araki, Effect of silicon content on densification, mechanical and thermal properties of Al-xSi binary alloys fabricated using selective laser melting, Mater. Sci. Eng. A 682 (2017) 593–602.
[14] G. Liu, G. Li, A. Cai, Z. Chen, The influence of Strontium addition on wear properties of Al–20 wt% Si alloys under dry reciprocating sliding condition, Mater. Design 32 (1) (2011) 121–126.
[15] P. Ma, K.G. Prashanth, S. Scudino, Y. Jia, H. Wang, C. Zou, Z. Wei, J. Eckert, Influence of annealing on mechanical properties of Al-20Si processed by selective laser melting, Metals (2014) 28–36.
[16] M. Mueller, M. Riede, S. Eberle, A. Reutlinger, A.D. Brandão, L. Pambaguian, A. Seidel, E. López, F. Brueckner, E. Beyer, C. Leyens, Microstructural, mechanical, and thermo-physical characterization of hypereutectic AlSi40 fabricated by selective laser melting, J Laser Appl. 31 (2) (2019) 022321.
[17] C.E. Roberts, D. Bourell, T. Watt, J. Cohen, A novel processing approach for additive manufacturing of commercial aluminum alloys, Phy. Proc. 83 (2016) 909–917.
[18] M. Simonelli, N.T. Aboulkhair, P. Cohen, J.W. Murray, A.T. Clare, C. Tuck, R.J. Hague, A comparison of Ti-6Al-4V in-situ alloying in selective laser Melting using simply-mixed and satellited powder blend feedstocks, Mater. Charact. (2018) 118–126.